Journal of Remote Sensing
A SCIENCE PARTNER JOURNAL

RESEARCH ARTICLE

Simulating Potential Tree Height for Beech–Maple–Birch Forests in Northeastern United States on Google Earth Engine

Zhenpeng Zuo*, Luofan Dong, Yuri Knyazikhin, and Ranga B. Myneni

Department of Earth and Environment, Boston University, Boston, MA, USA.

*Address correspondence to: zpzuo@bu.edu

Citation: Zuo Z, Dong L, Knyazikhin Y, Myneni RB. Simulating Potential Tree Height for Beech–Maple–Birch Forests in Northeastern United States on Google Earth Engine. *J. Remote Sens.* 2023;3:Article 0084. https://doi.org/10.34133/remotesensing.0084

Submitted 21 March 2023
Accepted 5 September 2023
Published 9 October 2023

Copyright © 2023 Zhenpeng Zuo et al. Exclusive licensee Aerospace Information Research Institute, Chinese Academy of Sciences. Distributed under a Creative Commons Attribution License 4.0 (CC BY 4.0).

Estimating potential height of forests is one of key tasks in forest restoration planning. Since regional maximum height statistics is difficult to account for local heterogeneity, biotic and abiotic mechanism-based methods are required. Different from the mainstream models that possesses either hydraulic constraint or mechanical constraint, we used a more lightweight model based on balance of water availability and consumption, named the Allometric Scaling and Resource Limitations model. Several enhancements were added, making up the third version of the model, and we deployed it using Google Earth Engine (GEE). A map of potential tree height at 90-m resolution is created for beech–maple–birch forests in northeastern United States. Within the oldest forests among the study area, the model reproduces the tree height level of ~25 m with root mean square deviation (RMSD) of 3.71 m from a high-resolution product of canopy height estimates. Under a threshold of 20% deviation, 82.9% of pixels agree with the existing tree heights. Outside of the oldest forests, RMSD raises to 5.01 m, and agreement drops to 75.3%. Over the entire study area, 6.6% total pixels of interest have a predicted height below the current level. A total of 16.7% pixels have larger predictions relative to existing forest heights, with a half of them classified as mistakes of overestimation. Errors may come from uncertainty in climate reanalysis data and inadequate shading effects modeling. Our work confirms the applicability of this lightweight model for this static prediction task and explores the deployment of ecological mechanism-based models on the GEE platform.

Downloaded from https://spj.science.org on October 14, 2023

Introduction

Tree height is considered as an important indicator to quantify forest maturity [1]. It also serves as a good predictor for dry mass and allocation, productivity, energy budget, water fluxes, and biodiversity [2–7]. Potential tree height, the upper limit canopy height that a stand (assuming constant plant species and climate conditions) can reach in the future with the growth over an infinite timeline, represents the ultimate size scale of a species under local geographic conditions and may infer magnitudes of a series of quantities that are important to carbon and water cycles of an ecosystem. Grounded on this, predicting potential tree height becomes a spot of interest in understanding future forest development and structure, which is of profound significance for forest restoration planning and evaluation [8].

Stand-level maximum is observable and can be used as a surrogate for potential tree height if the observed trees are mature. However, faced with the problem of assessing site-specific potential tree height, a purely observational approach is not appropriate. Forest inventory [9] and space-borne light detection and ranging systems [10] can provide as accurate measurements of tree height as possible, but these data are usually sparse and therefore fail to capture strong variability at small spatial scales. Moreover, strong impact of site-dependent biotic (e.g., physiology) and abiotic factors (e.g., climate, terrain, and soil) on local tree height (as discussed by Fricker et al. [11]), may not be captured by the statistics-based maximum tree height estimates.

With the advancement in computer simulations of forest processes at various scales, several mechanism-based models for simulating potential tree height emerged. The concept is generally described as an explicit or implicit function of external environmental conditions, such as climate and topography. Allometric laws are used to measure the scaling relationships between dimensions of tree segments [7], and hydraulic and mechanical constraints are the most accepted mechanisms [12]. The hydraulic constraint assumption, which is more commonly used, states that the increase in water transport resistance with height growth will lead to stomatal contraction/closure and therefore slows down the growth [13–15] and that the maximum height can be found at zero net productivity. Derived from this, some methods also consider tree's adaptation to hydraulic constraints, such as actively adjusting the allocation of dry mass in leaf tissue and stem at each height to maximize growth rate [16]. Another dimension is provided by the mechanical constraint assumption, which states that the gravitational stress at tree base increases with height until tree bends from vertical under its own weight [17], as does the possibility of mechanical damage [18]. There is still debate as

to which mechanism is the most critical determinant of the potential tree height around the world [19].

Complementary to the hydraulic constrain model but being fundamentally different in approach, Kempes et al. [20] proposed a simple but effective model for prediction of potential tree height based on allometry and water limitations, namely the Allometric Scaling and Resource Limitations (ASRL) model. In this model, a tree is in a favorable water status if its actual stem flow rate (i.e., transpiration) does not exceed the maximum water acquisition rate of roots and is greater than the minimum rate to support life. The potential tree height occurs at the boundary of this favorable status. The rates of transpiration, maximum root acquisition, and minimum life-sustaining flow are separately associated with dimensions of crown, root, and stem, which are quantitatively deduced through allometry from tree height. Different from the hydraulic constraint model, it does not simulate stomatal behavior that vary with leaf water stress; rather, an empirical, constant stomatal opening is used for each tree height. The simplicity attracted testing in multiple landscapes ranging from country to regional levels [21–26]. They demonstrated that a set of values for the model parameters could always be found in the parameter space so that the tree height predictions of the model could approximate the current or target tree height. However, there has been very little effort to make use of the model without performing parameter tuning tactics. Here, we modified and tested the model's ability to predict potential tree heights for the beech–maple–birch (BMB) forests in northeastern United States. A 90-m map with satisfactory accuracy is made public along with this work, hoping to assist forest restoration planning.

Materials and Methods

Experimental design

History of the ASRL model

Kempes et al. [20] proposed the ASRL model to simulate basal demand, absorption availability, and evapotranspiration (ET) of trees for water, which are increased under different rates with growth, and to calculate the potential tree height by searching for equilibrium of the 3 flow rates according to the geospatial conditions. The model deploys a conceptual tree, which is generalized using averaged parameters across species, topographic conditions, and climatological gradients. Without competition or mutual shading, the conceptual tree's growth limit is sorely determined by the biophysical context, and its maximum height can therefore be predicted with a finite number of environmental factors.

The ASRL model framework contains 3 modules corresponding to 3 water flows respectively, each of which can establish an explicit function with tree height. The basal demand module models the relationship between the metabolic minimum requirement of water flow (Q_0) and tree height (h) based on allometric laws between flow rate and stem diameter (D) and h (Eq. 1). The ET module models the ET rate (Q_e) of crown with respect to h based on the Penman–Monteith equation as well as allometric scaling of the component variables (e.g., absorbed radiation, R_{abs}, and effective areas, $a_{S,L,T}$, for fluxes of sensible heat, latent heat, and thermal emission) and the climate that regulate the flow of ET (simplified in Eq. 2). The absorption availability module models the maximally available water intake (Q_p) by roots with respect to tree height based on precipitation P, allometry of root size $r_{root}(h)$, and an invariant root absorption efficiency γ (Eq. 3). The ASRL model in its entirety attempts to solve for intersections of each pair of the 3 flow rates to evaluate the steady state of demand, intake, and dissipation. So, the potential tree height is picked from the intersection points which represent the boundary of tree's favorable water status.

$$Q_0(h) = \beta_1 D^{\eta_1} = \beta_2 h^{\eta_2} \tag{1}$$

$$Q_e = f\left(R_{abs}, a_{S,L,T}, \text{climate}\right) \tag{2}$$

$$Q_p(h) = \gamma \pi \left[r_{root}(h)\right]^2 P \tag{3}$$

In the subsequent development, Choi et al. [23] deployed multiple modifications to the ASRL model that constituted the second version. That version was designed to construct a data product of existing tree heights in the era when there had not been many data-driven ones to choose from. This effort necessarily changed the meaning of the model from predicting future levels into fitting the current. To force the model to align with the current height references, Choi et al. [23] performed an iterative optimization for some tree traits (coefficient β_1 in the tree height-stem diameter allometry, root water absorption efficiency γ, and single leaf area s_{leaf}) by ecoregion and by species group. The data-driven parametric optimization markedly enhanced the model's capability to capture spatial heterogeneity between landscapes. However, this practice weakened the prognostic nature of the model and did not guarantee that the searched parameter values, which drove the predictions to fit the target heights, also held true in reality. An example of unrealistic searched values was that the single leaf area for needleleaf/mixed forests in northeast United States was approximately 2 orders of magnitude larger than that of the nearby deciduous broadleaf forests (see Fig. S3 of [23]).

Aside of the parameter tuning design, some technical details were also modified in the second version to enhance the model. Time scale of calculating Q_e and Q_p was increased from annual (i.e., the flows were calculated with an average annual climate) to monthly (i.e., the flows were calculated with long-term average monthly climate then summed up), which improved the temporal precision of the model. This also gave the model some ability to rule out contribution of weather during nongrowing periods, such as winter. Using a monthly mean temperature of 5 °C as the threshold, low-temperature months were excluded when adding up the annual Q_e and Q_p.

The second version also improved the way of tree parameterization, which originally was using multispecies average traits to generalize trees. In order to consider interspecific and regional variations, Choi et al. [23] compiled allometric relationships of stem diameter versus tree height and of crown size (crown height and width) versus tree height per class of region and species group, using multiyear in situ measurements from the Forest Inventory and Analysis (FIA) database. Tree height in this version is no longer sorely determined by the environment but is also regulated by the measurement-based parameterization, which reflected some region-specific morphological effects of tree's interactions (such as competition and shading) in forests.

As of modification of mechanisms, the second version changed the scale of water flux simulation. The ET module was built upon

Downloaded from https://spj.science.org on October 14, 2023

the Penman–Monteith equation, which normally models the canopy as a big leaf [27]. However, in the original version, the Penman–Monteith equation was used in a nonstandard way, calculating water flux at the level of leaf surface area. The water flux per unit leaf area was then upscaled to crown level using total leaf area, assuming energy fluxes are consistent throughout the crown. In the second version, instead, the big-leaf approach was adopted, and the expression of area was naturally changed to canopy projection area (i.e., ground area). The effective areas introduced for energy fluxes in Eq. 2 were abandoned.

A terrain correction was introduced into the absorption availability module. In the original model version, only precipitation, root size, and root absorption efficiency were included for deriving the upper limit of water uptake. As an improvement, Choi et al. [23] adopted the topographic wetness index (TWI), normalized by extreme values, as a multiplier of precipitation, considering that 2 terrain-induced opposite effects, water catchment and water runoff, may have impacts on water availability. TWI is the logarithm of ratio of specific catchment area (total catchment area per unit length of contour line) to local terrain slope [28], which describes the water retention capacity driven by topography, and can be taken as a proxy of soil moisture [29]. Therefore, Q_p module of the second ASRL version applied an upgraded formula (Eq. 4),

$$Q_p(h) = \gamma \pi \left[r_{root}(h)\right]^2 P \Psi \tag{4}$$

where Ψ denotes the maximum-normalized TWI.

Model improvements in this work

In this study, we proposed the third version of the ASRL model aiming at predicting potential tree height (Fig. 1) to help delineate forest restoration opportunities, and deployed it on the new-born geospatial cloud computation platform Google Earth Engine (GEE). Considering the prognostic nature of potential height prediction, we did not repeat the parametric tuning scheme. However, we reserved many contributions of Choi et al. [23] to the model and explored some further improvement dimensions.

Our third generation of ASRL model is optimized at time scale, spatial resolution, and model mechanisms. The time scale of the modules was further increased to a day-of-year DOY level (that is, the Q_e and Q_p flows per DOY were calculated based on average daily climate and then summed up). The spatial resolution was increased from 1 km in the work of Choi et al. [23] to 90 m, allowing the model to capture finer spatial heterogeneity of the terrain. Input data with more sparse resolutions were bicubically resampled to 90 m during preprocessing.

We prudently removed the module for Q_0, the so-called minimum basal demand of water flow, leaving only Q_p and Q_e to participate in the model. We found no evidence in the literature that flow Q_0 based on Eq. 1 can be defined as the minimum water flow demand of plants, which implies a situation where plants will die if the actual water flow falls below the demand. Instead, it is commonly used as a stem flow rate estimate under empirical multispecies regression [30,31], and flow rate being lower than the regression value is allowed. Early results (Fig. S4) shows the $Q_0 - Q_p$ intersections and the $Q_0 - Q_e$ intersections deviate largely from existing canopy height estimates as well as the $Q_p - Q_e$ intersections (used as the ASRL v3 predictions). Seen as the minimum demand estimates, the Q_0 module may weaken the simulation both theoretically and quantitatively.

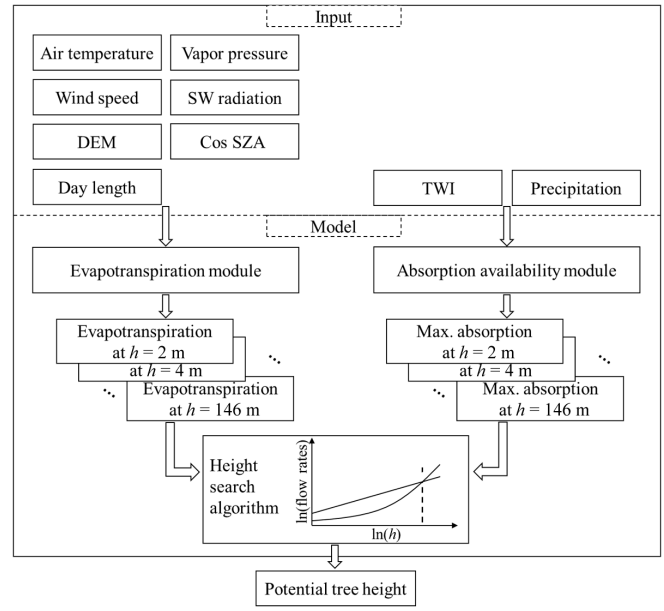

Fig. 1. Flowchart of the proposed Version 3 of the ASRL model for potential tree height prediction. Air temperature, vapor pressure, wind speed, SW radiation, and precipitation are given as 10-year averages for each day of year (DOY). Cosine of solar zenith angle (cos SZA, daily average) and day length are generated at the DOY level. The ET module (for Q_e) and absorption availability module (for Q_p) first perform calculation of the flows at daily scale then sum up to annual scale.

As an important part of the Penman–Monteith equation, a correct estimation of the absorbed shortwave (SW) radiation is key to ensure the accuracy of the model. We referred to the discussion of Campbell & Norman [32] on canopy optical properties, which opposed using an average transmittance (or reflectance) to both visible and near-infrared (NIR) radiation segments when calculating the SW transmittance (or reflectance) of the canopy. In the first 2 versions of the ASRL model, such unrecommended approach was used. To get a better estimate of canopy absorptance, our version calculated transmittance and reflectance for visible and near-infrared separately. The calculation of transmittance, reflectance, and the derived absorptance were also performed at the DOY level. Information of solar altitude required to calculate extinction coefficients was provided by a site-specific daily mean cosine of solar zenith angle (cos SZA).

In the absorption availability module, we retained the normalized TWI (Ψ) as the terrain correction term. A new effect was also considered in this study in addition to the topographic effect, which is the constraint of stem flow rate due to growth-induced increment of water transport distance. In other words, increasing tree height per se extends water transport distance and hydraulic resistance, thus restrains the flow. This effect was not considered in the simplistic root modeling of the previous versions, which assumed water availability increasing geometrically with tree height due to extended root size (Eqs. 3 and 4). Knowing an overestimation of water accessibility can lead to excessive estimates and uncertainty of potential tree heights, we modified the module to account for the hydraulic restraining effect without completely overturning the prior model structure (see below).

Our hydraulic restraining modeling aims to reflect how tree height increment may restrain water availability. The previous

Downloaded from https://spj.science.org on October 14, 2023

version of potential (maximum) water flow a tree at h can absorb from the environment (i.e., Q_p in Eq. 4, hereafter $\widetilde{Q_p}$) considered intrinsic tree properties (expressed as a constant absorption efficiency, γ), root size with respect to h, (as root radius, $r_{root}(h)$), total water in the environment (as precipitation, P), and terrain correction (normalized TWI, Ψ), and used a multiplication to assemble the factors together (Eq. 4). When this old modeling is revisited under the case of hydraulic restraining effect, $\widetilde{Q_p}$ can be viewed as that under an invariant hydraulic restraining effect at a certain tree height $\widetilde{h}$. To enable the effect to vary with h, our reconstructed Q_p should be taken as the ratio of $\widetilde{Q_p}$ and the $\widetilde{h}$-normalized tree height $\frac{h}{\widetilde{h}}$, i.e.,

$$Q_p(h) = \widetilde{Q_p} / \frac{h}{\widetilde{h}} = \gamma \pi \left[r_{root}(h)\right]^2 P \Psi \frac{\widetilde{h}}{h} \quad (5)$$

Early tests confirmed that setting $\widetilde{h}$ at 25 m, which is the approximate potential height that trees of the species group can reach, yielded overall reasonable predictions. Varying this parameter does not cause large perturbation to the model output (see sensitivity analysis in Results).

We continued the practice of using the FIA and the Forest Health Monitory (FHM) databases (see Data) to extract the key allometric scaling relationships. The coefficients and exponents of the relationships (tree height versus stem radius, tree height versus crown height, and tree height versus crown radius) were extracted under log-log regression for the species group of interest.

Implementation on GEE

The program of the model was written using the GEE Python API. Nine processing functions (Table 1) were included, covering calculation of the 3 water flow rates, and a search algorithm for finding intersections among any of the flows. Main functions of the 3 flow rates (Functions 1, 2, and 8) were written in a way of an output image (ee.Image object) given a single input tree height (ee.Number object). Specially, the ET module (Function 8) contained 5 subfunctions (Functions 3 to 7) to derive canopy attributes and energy balance variables based on allometric relationships and meteorological conditions. As the outputs, the multichannel flow rate raster images were constructed from multiple discrete tree height candidates, each channel denoting the corresponding water flow rate at a given tree height candidate. Based on the 3 flow rate images, the search algorithm finally calculated at pixel level the tree heights where the flow rate curves intersected.

Function of the search algorithm solving for intersection tree heights for flow rate curves was named "findAsrlHt" (Function 9), taking the 2 multichannel raster images as inputs. For each h interval sandwiched by 2 neighboring h candidates, the function linearly solved for a meeting point based on the flow values at the 2 endpoints. If a calculated meeting point for an h interval at a pixel did not fall into the interval, it would be ruled out by an image mask. Interval by interval, the linear intersection searching algorithm would extract all h-interval-based linear intersections throughout the feasible range of tree height (2 to 146 m). The function finally returned the summarized intersections between Q_p and Q_e for all pixels as a raster image (ee.Image object). Satisfying $Q_e < Q_p$ at a small tree height (2 m), which holds for every pixel in the study region, the ASRL-derived potential tree height allowed by biogeophysical conditions was taken as the minimum value of intersections between Q_p and Q_e.

Table 1. Processing functions of ASRL.

	Name	Functionality
1	genQ0Rate	Generate a Q_0 raster at a given h following Eq. 1 (not used)
2	genQpRate	Generate a Q_p raster at a given h following Eq. 5
3	calcCroGeom	Calculate crown leaf number and crown size at a given h
4	calcAbsRad	Calculate daily crown absorbed radiation flux at a given crown setting
5	calcCoefTher	Calculate h-independent daily coefficients for outgoing thermal flux
6	calcCoefSens	Calculate daily coefficients for outgoing sensible heat flux at a given h
7	calcCoefLatn	Calculate daily coefficients for outgoing latent heat flux at a given h
8	genQeRate	Generate an annual-summed Q_e raster at a given h based on the Penman–Monteith equation, calling Functions 3 to 7
9	findAsrlHt	Solve for intersection h between $Q_p(h)$ and $Q_e(h)$

The model contained a preprocessing function that ran before the processing functions. The preprocessing resamples the meteorological reanalysis data so that the model can work on the more refined DEM grids (90-m resolution). In addition, the preprocessing function generates other necessary variables for the model, such as vapor pressure based on dew point temperature.

Data

Study region We conducted experiments in the BMB deciduous forests, which are widely distributed in the northeastern United States. The study region (66°W to 80°W, 40°N to 48°N, excluding water areas and Canada) contains New England, New York, and the majority of Pennsylvania, where the BMB forests predominate (Fig. 2A). According to Ruefenacht et al. [33], area of the BMB forests in the study region is 1.7×10^7 ha (42.4% of total land area). In addition to the BMB forests, major forest groups also include the spruce–fir group (7.6%) in New England and the oak–hickory group (13.7%) in the south. The Ruefenacht et al. [33] data were used to generate a BMB forest mask. To ensure correctness of forest type classification, we also applied a deciduous forest mask retrieved from the NLCD 2019 land cover database [34] in addition to the BMB mask although the 2 datasets may have disagreement. It is because Ruefenacht et al.[33] reported their forest type group data had an overall accuracy of only 63% to 67% in our study area. The deciduous forest layer was introduced as an enhancement to avoid confusion of including a de facto conifer forest, which

Downloaded from https://spj.science.org on October 14, 2023

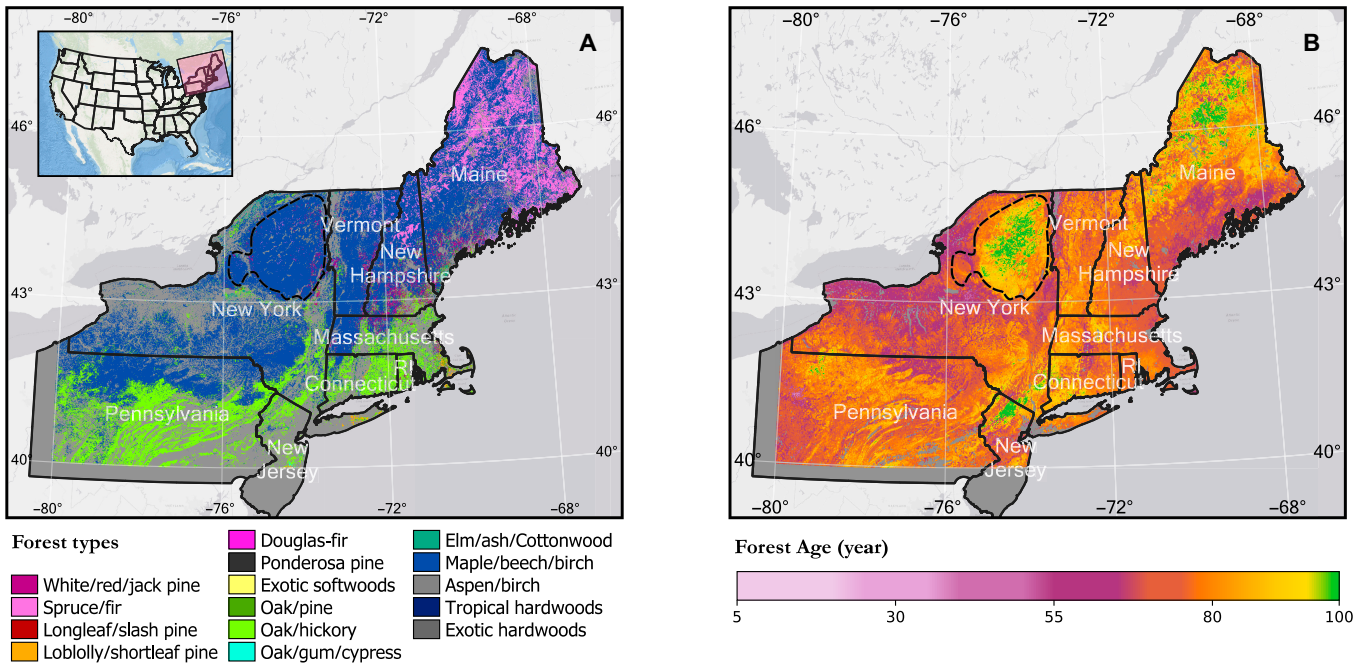

Fig. 2. Spatial distributions of (A) forest groups [33] and (B) forest age [36] in the study region. The dashed circle outlines the mature forest area in upstate New York (Ecoregion M212D) where allometric relationships were extracted and where the evaluation will primarily be focused. State names are labeled (the acronym "RI" stands for Rhode Island). In Panel A, the BMB group is rendered as dark blue, and the 2 submajor forest groups took light green (oak–hickory group) and light pink (spruce–fir group). In Panel B, a nonlinear color scheme is applied to emphasize old forests of >80 years age.

is also a common tree type in the area. Applying the second mask reduced the total forest area of interest to 7.25×10^6 ha.

The Warm Continental Regime Mountains ecoregion (coded M212D in [35]; dashed circle in Fig. 2) that spatially overlaps Adirondack Park (established in 1892) is contained in the study area, which is home to multiple preserved lands thus possesses spatially continuous BMB forests free from large-scale land use. The forests in Ecoregion M212D have the longest age (>80 years for the vast majority pixels, Fig. 2B) among the neighboring lands [36]. Therefore, we consider this area the mature forests. Tree height estimates in this ecoregion will serve as the primary standard for evaluating the ASRL potential height predictions. In addition, the main parameters of the model are derived from field measurement data in the ecoregion. Area outside Ecoregion M212D is used as the validation region to evaluate the model's possible dependence on region-specific parameterization, which can be a possible factor weakening the performance. Model predictions in the validation region are also provided.

Topography For elevation, we used the 90-m HydroSHEDS v1 void-filled DEM dataset [37], which was derived from the 90-m SRTM elevation product with removal of spikes and sinks and served as the topographic basis for other HydroSHEDS products. As a preprocessing, we reprojected the void-filled DEM to the grids under a projection coordinate system at a resolution of 90 m, which was then used as the resolution baseline of reprojection for subsequent data layers. The meteorological reanalysis data in the following parts will be resampled aligning to the 90-m grids before input. The void-filled DEM was also used to generate a map of slope for the study region.

The normalized TWI, Ψ, a multiplier of precipitation in the Q_p module, was derived from the HydroSHEDS hydrologically conditioned DEM dataset. Following the workflow from Mattivi et al. [38], we used an open source software SAGA GIS (version 7.8.2) and ran the Flow Accumulation (top-down), Flow Width and Specific Catchment Area, and Topographic Wetness Index tools in sequence to obtain the TWI. Ψ was then calculated by a maximum normalization, i.e., dividing TWI by its maximum level (≈16) observed in the study region.

Climate To model potential, steady-state canopy height with wall-to-wall coverage, our experiment set up a climate condition using a combination of 2 GEE-cataloged, gridded meteorological reanalysis datasets. The 2.5-km Real-Time Mesoscale Analysis (RTMA 2.5, referred to as RTMA for simplicity) [39], supported by National Oceanic and Atmospheric Administration (NOAA), has hourly simulations for the contiguous United States (CONUS) since 2011. The 1-km DAYMET dataset provides a daily average of climate simulations across the globe since 1980 [40]. The model variables for temperature, humidity, and wind were provided by the RTMA dataset, and the variables for precipitation and SW radiation were provided by DAYMET (Table 2).

We used the meteorological reanalysis datasets of 10 years (2011 to 2020) to establish climate grids for every DOY. To meet the daily time scale of the modified ASRL model, the 3 hourly RTMA variables (temperature, vapor pressure, and wind speed) and a daily DAYMET variable (SW radiation) should be taken as the daytime average per DOY. For this purpose, we developed a preprocessing step to reduce the daily or hourly data into such DOY daytime mean. First, a set of temporal filters working on image metadata organized the images of 2011 to 2020 by DOY. Second, for the 3 RTMA variables, grids within the nighttime areas were ruled out based on timestamp of the image and the sunrise/sunset hours of DOY, while only the daytime data were retained. As for the DAYMET variable, SW radiation, it did not require a day/night mask in that it had already been given as the average over the daylight period in the source dataset (Table 2). Then, the 4 preprocessed variables

Downloaded from https://spj.science.org on October 14, 2023

Table 2. Core climate variables for ASRL v3.

Variable name	Source	Unit	Original frequency	Notes
Air temperature	RTMA	°C	Hourly	—
Vapor pressure	RTMA	kPa	Hourly	Converted from RTMA dew point temperature in °C following the Tetens equation
Wind speed	RTMA	m/s	Hourly	—
Precipitation	DAYMET	mm/day	Daily	—
SW radiation	DAYMET	W/m^2	Daily	Taken as average over the daylight period of the day

of the ET (Q_e) module took their respective mean values on each of the 365 DOYs. For precipitation used in the water availability (Q_p) module, we directly used the temporal-filter-organized, 10-year collection to calculate the DOY mean.

Traits and allometry We used the in situ measurements of FIA and FHM databases to retrieve 3 sets of allometric scaling relationships: (a) tree height versus stem radius, (b) tree height versus crown height (vertical length of crown), and (c) tree height versus crown radius. Among them, relationships a and b were retrieved from the FIA database, whereas relationship c was from the historical FHM database since the crown diameter measurements were not performed in the FIA Program. To retrieve allometric relationships of mature forests only, we restricted the spatial scope of the data to counties whose land area are completely or mostly within the Ecoregion M212D (see also Fig. 2) in upstate New York. Data records of unrelated tree species or groups were filtered out by field key searching. Duplicate records of same trees spanning multiple years were screened by keeping the record of the last year only. The allometric relationships were obtained by log-log regressions, so that the exponential term of an allometry corresponded to the regression coefficient, and that the coefficient term of the allometry was equal to the exponent of the regression offset.

Single leaf area (s_{leaf}) and root absorption efficiency (γ) are 2 important parameters and were included in the parameter tuning steps of the second model version [23]. In this version, we used constant values for them as we abandoned the parameter tuning tactics. For s_{leaf}, 30 cm^2 was used, which was the average of multiple BMB species in the TRY database [41–45]. For γ, we used 0.12 (dimensionless), which was a calibrated value based on FIA tree height records of Ecoregion M212D counties, in reference to the calibration method provided by the first model version [20]. First, tree records of the tallest 5% trees in the counties of interest were extracted from the FIA tables. Second, for each tree record, we searched for a γ value that made the intersection point of Q_0 and Q_0 curves to fall exactly at the tree's height. Finally, all the tree-specific γ values were averaged to obtain the module-wise constant parameter value. In the above steps, site-specific TWI at the trees' positions on which the Q_p module relies were given as the county-level average TWI, in that the FIA data hid the real spatial coordinates [9].

Model evaluation

The evaluation of the model predictions was mainly based on comparisons with existing tree height estimates. In recognition of the limitation of such comparison that the current tree height might not have as tall level as the environment allowed, we mainly looked at the model's performance on sufficiently tall forests and selectively ignored sites where real tree heights unlikely reach tall levels. Model evaluation was conducted in 2 regions separately: (a) Ecoregion M212D of continuous wild forests, in which the core traits and allometry were retrieved, and (b) the validation region, i.e., everywhere else in the study region. We compared the model's predictions with tree height products at pixel level and with FIA field measurements at county level.

Comparisons with canopy height products

We compared the results with 3 raster GIS datasets of existing tree height, with a primary focus on the performance in Ecoregion M212D which is mostly protected forests. GEDI L3 product is a 1,000-m aggregation of GEDI-sampled canopy height observations. Potapov et al. [46] provide a 30-m, full-coverage tree height estimation for year 2019 based on a GEDI-Landsat data fusion. Lang et al. [47], which self-reported higher accuracy than the Potapov dataset, provides a 10-m tree height estimation for year 2020 based on a GEDI-Sentinel data fusion. To compare at the model's resolution (90 m), the 1,000-m GEDI L3 data were resampled bilinearly, and the 30-m Potapov and 10-m Lang data were reduced in a way of averaging. We used 3 statistical metrics to measure deviations between the model and the existing height estimates–mean deviation (MD, Eq. 6), root mean square deviation (RMSD, Eq. 7), and mean absolute deviation (MAD, Eq. 8). We spotted where the model failure occurred using an acceptance threshold of ±20% deviation from the newborn, high-accuracy Lang estimates.

$$\mathrm{MD} = \frac{1}{n}\sum_{i=1}^{n} \mathrm{ASRL}_i - \mathrm{Ref}_i \tag{6}$$

$$\mathrm{RMSD} = \sqrt{\frac{1}{n}\sum_{i=1}^{n} \left(\mathrm{ASRL}_i - \mathrm{Ref}_i\right)^2} \tag{7}$$

$$\mathrm{MAD} = \frac{1}{n}\sum_{i=1}^{n} \left|\, \mathrm{ASRL}_i - \mathrm{Ref}_i \,\right| \tag{8}$$

A postprocessing of screening was performed to remove the impact of immature forests on our model evaluation. That is, we would check whether the existing forests have simply not grown tall enough yet, or it was the potential tree heights per se that were overestimated. We believed that immature forests would show a trend of growth, therefore, we used a

Downloaded from https://spj.science.org on October 14, 2023

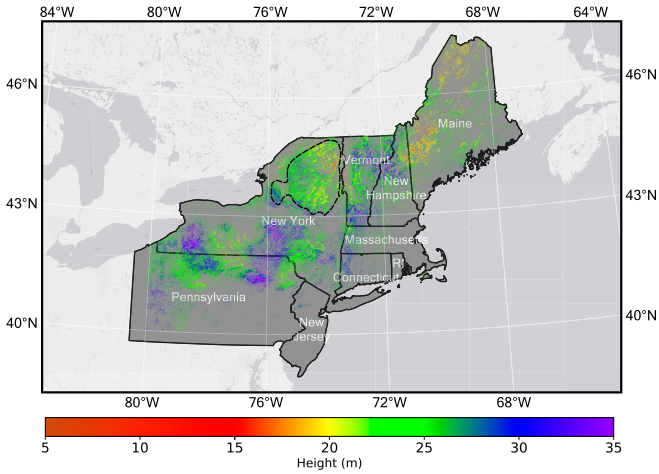

Fig. 3. The ASRL model predictions on potential tree height over the study region (90-m grids) for BMB forests. A combined mask created with conditions of BMB forest group and deciduous forest land cover was used to rule out irrelevant pixels. The dashed circle outlines Ecoregion M212D.

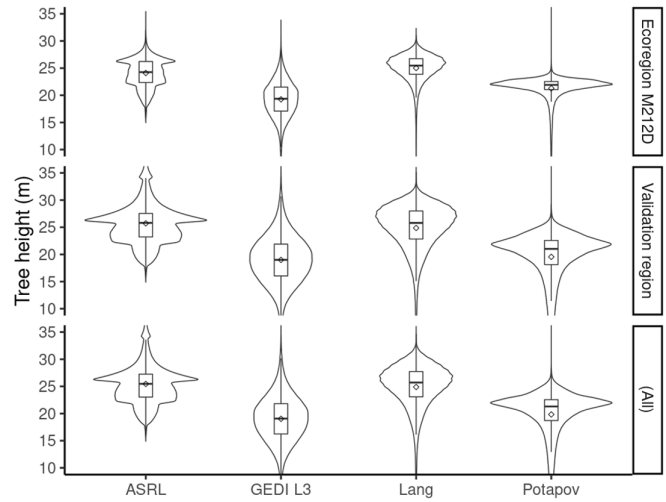

Fig. 4. Pixel-level distributions of ASRL potential height, GEDI L3, and data-fusion products of Potapov et al. [46] and Lang et al. [47] in Ecoregion M212D and the validation region. Graphs in each region are scaled to have the same area. Boxplots in the graphs shows the first and third quartiles (box edges), median values (central horizontal line), and mean values (diamond).

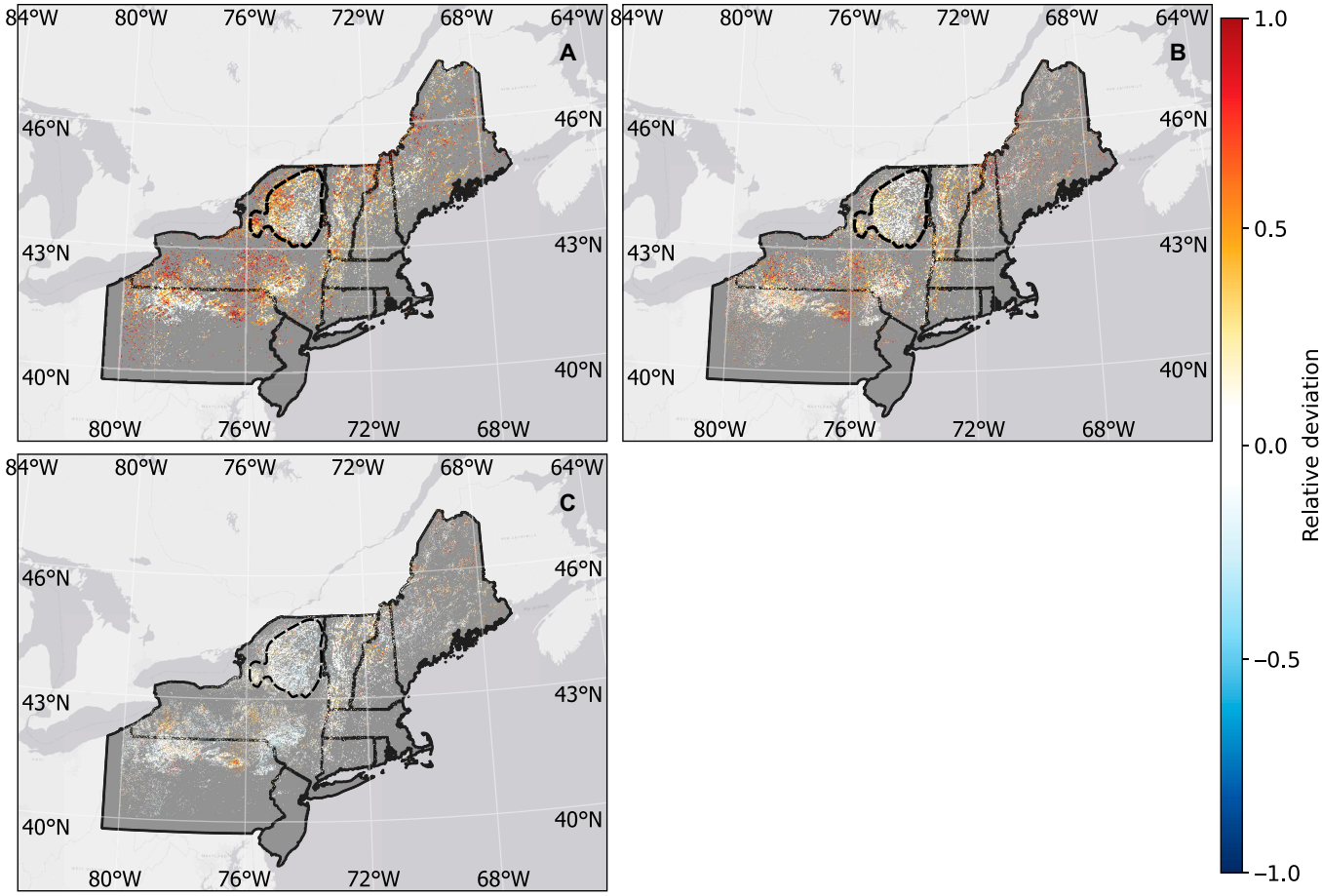

Fig. 5. Relative deviation (= (ASRL−Ref) / Ref) of the ASRL potential tree height from (A) GEDI L3, (B) Potapov et al. [46], and (C) Lang et al. [47]. Image mask used to generate this figure was same as that for Fig. 3.

trend detection tool to generate a trend mask for the potential tree height map. Using a harmonic fitting-based model for Landsat observations (Continuous Change Detection and Classification [CCDC] [48,49]; see also Supplementary Materials), we located a group of pixels that have a long-term trend of normalized difference of fraction index (NDFI). The CCDC algorithm

Downloaded from https://spj.science.org on October 14, 2023

Table 3. Comparisons of ASRL potential tree height predictions to existing tree height products.

	Region	MD (m)	RMSD (m)	MAD (m)
ASRL versus GEDI L3	Ecoregion M212D	4.83	6.51	5.42
	Validation region	6.73	8.51	7.12
	Overall	6.41	8.21	6.84
ASRL versus Potapov et al. [46]	Ecoregion M212D	2.82	4.52	3.46
	Validation region	6.17	8.41	6.40
	Overall	5.61	7.90	5.91
ASRL versus Lang et al. [47]	Ecoregion M212D	−0.91	3.71	2.94
	Validation region	0.86	5.01	3.70
	Overall	0.56	4.82	3.57

diagnosed NDFI time series on a pixel-by-pixel basis and detected inter-annual trend and intra-annual seasonality of spectral bands or indices by harmonic fitting. We established the no-trend mask based on a threshold of pixel-specific maximum time series slope. Technically, we first used the CCDC algorithm to obtain all the time series segments (allowing up to 8 segments for each pixel), and then saved the maximum NDFI slope of the segments for each pixel. If the maximum slope exceeded $\pm 5 \times 10^{-3}$ NDFI per year, the pixel would be gotten rid of.

Comparisons with FIA field measurements

We also compared the ASRL predictions with the tree height measurements from the FIA database. Previously, we used FIA as the source of the allometric scaling parameters in our model-it was used during model construction to extract the allometries without revealing local tree height levels. Although the FIA database provided latitude–longitude coordinates for sampled plots, the coordinates did not refer to true locations because a fuzzing and a swapping processing altered them to protect landowner's privacy. The alteration made it impossible to evaluate the model in situ, so we instead turned to county-level evaluation. Median ASRL predictions were compared to average height of the tallest 5% BMB trees of FIA records in every county.

Results

The model is deployed on GEE in BMB broadleaf forests in the northeastern United States to predict tree height potential based on current climate conditions. This 90-m-resolution tree height potential dataset enables providing insights into forest growth potential and can be useful for forest restoration assessment. The entire domain covers a total of 7.2×10^6 ha area (≈9 million non-null pixels) of the BMB deciduous forests. Running all modules including the height searching algorithm used 22.6 million EECU-seconds in total, with the vast majority spent on the Q_e module (22.4 million, 98.9%).

A map of ASRL potential height predictions is created across the study area (Fig. 3). In Ecoregion M212D, the mean value of predicted tree height potential is 24.1 m, and the median is 24.3 m. In the validation region, the mean value of predicted tree height is 25.7 m, and the median is 25.8 m. Because the model used universal parameterization between the 2 areas, the predicted data in both regions have identical overall distribution (Fig. 4). In New York, Pennsylvania, Vermont, and New Hampshire, all outside of Ecoregion M212D, the model

Downloaded from https://spj.science.org on October 14, 2023

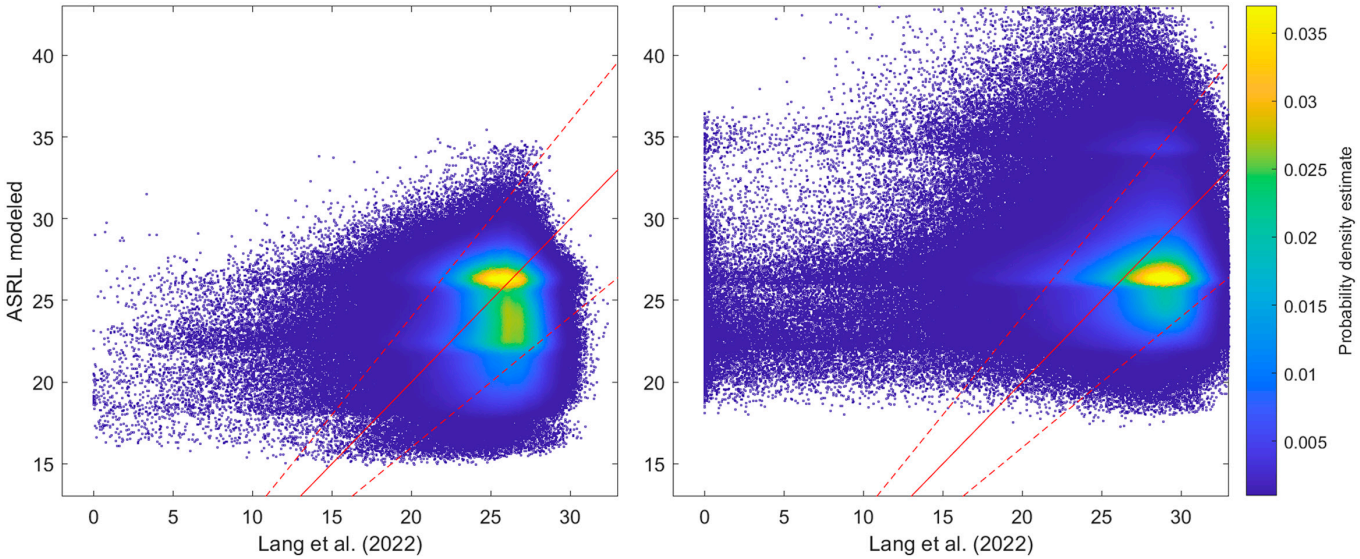

Fig. 6. Pixel-by-pixel comparison of ASRL potential tree height and Lang et al. [47] in Ecoregion M212D (left) and the validation region (right). All axes are in meters. Solid lines are the 1:1 line. Dashed lines indicate ±20% deviations. Data point colors indicate estimated kernel density.

reproduced local high levels as expected (blue to purple areas in Fig. 3), although some spots in those areas have overly high predicted values relative to the existing heights (dark red spots in Fig. 5C). Maine has the lowest level of potential tree heights among the study region and has very low values in some local spaces, which conforms to the high latitude and mountainous geography. In general, the model tends to predict higher tree height potential for locations further south or with less terrain slopes, and lower potential for locations further north or with higher terrain slopes.

To evaluate the model predictions, we looked at comparisons with existing tree height estimates including wall-to-wall canopy height products as well as field measurements. There are inconsistencies among the wall-to-wall products, but our predictions generally fall within the range outlined by the 3 distributions (Fig. 4) and agree more with the Lang et al. [47] product, which reports to have higher accuracy compared to other canopy height products, for most areas (Table 3, Figs. 4 and 5, and Figs. S2 and S3). The predictions have larger deviation from GEDI L3 and the Potapov et al. [46] products. Comparing to the Lang data alone, 82.9% valid pixels in Ecoregion M212D fall within the range of ±20% deviation, as do 75.3% pixels in validation region (Fig. 6). 6.5% (Ecoregion M212D) and 18.9% (validation region) pixels have > + 20% deviation from the Lang data. The model failed to reproduce tall enough results for 10.6% (Ecoregion M212D) and 5.8% (validation region) pixels (Fig. 6). For comparison with FIA field measurements, 169 counties (91.8% out of 185) fall within the range of ±20% deviations (Fig. 7).

Given the non-negligible areas (1.21×10^6 ha, or 1.5×10^6 pixels) where the predicted potential tree heights are substantially greater than the Lang estimates, we attributed those areas to (a) false error at immature forests and (b) real ASRL overestimation on potential heights using a trend analysis. Applying the CCDC-based trend mask, a large portion of high predictions are removed (Fig. 8C, compared to Fig. 4C). Their occurrence is mainly scattered and discontinuous, especially in Maine, and is very much correlated with ASRL excessive deviations (see examples in Fig. S1). In total, 5.4×10^5 ha areas (6.66×10^5 pixels, or nearly one-half) of the excessive positive deviation across the entire study region are masked out due to the trend. They point to the first explanation, that some positive deviations are simply because forests in the study area are not at their allowable peak height. They mark opportunities for forest restoration and highlight the application potential of our approach. However, the 4 areas of biased predictions in New York, Pennsylvania, Vermont, and New Hampshire in the validation region are not fully masked out, leaving the red-to-orange marked spots in the 4 states nearly unchanged (Fig. 8C). Not being masked indicated forests in those areas were mature enough. Therefore, the model is instead responsible for the prediction mistakes since it failed to fit to the local forest heights at these spots. 6.74×10^5 ha areas (8.3×10^5 pixels) with no CCDC-based NDFI trend can be classified as such model overestimations.

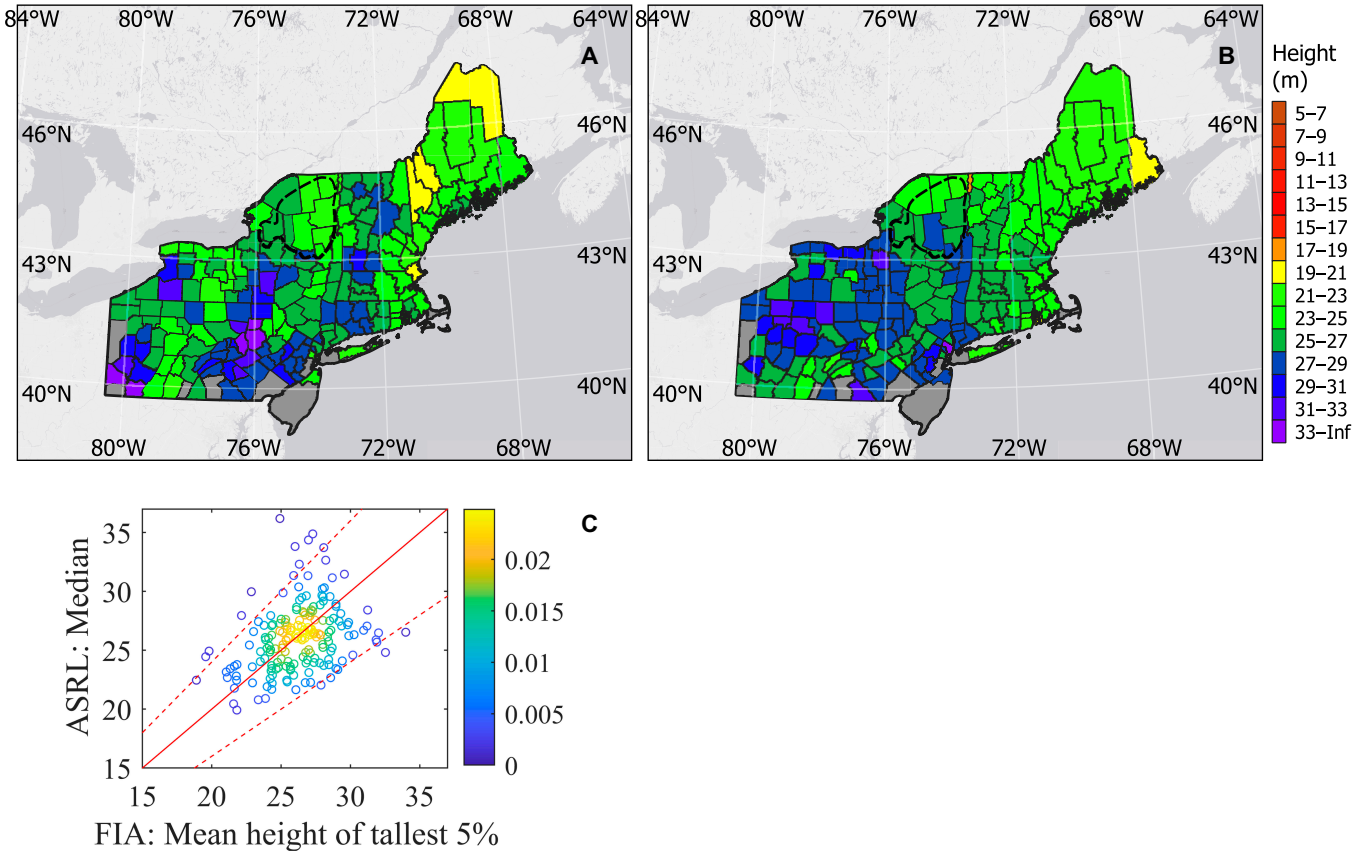

Fig. 7. County-level ASRL predictions and FIA records. One hundred eighty-four counties are involved (omitted 23 for limited ASRL pixels or FIA records). (A) County-level median ASRL potential tree height. (B) County-level FIA mean height of the tallest 5% trees. (C) County-by-county comparison. Both axes are in meters. Solid line is the 1:1 line. Dashed lines indicate ±20% deviations. Data point colors indicate estimated kernel density.

Downloaded from https://spj.science.org on October 14, 2023

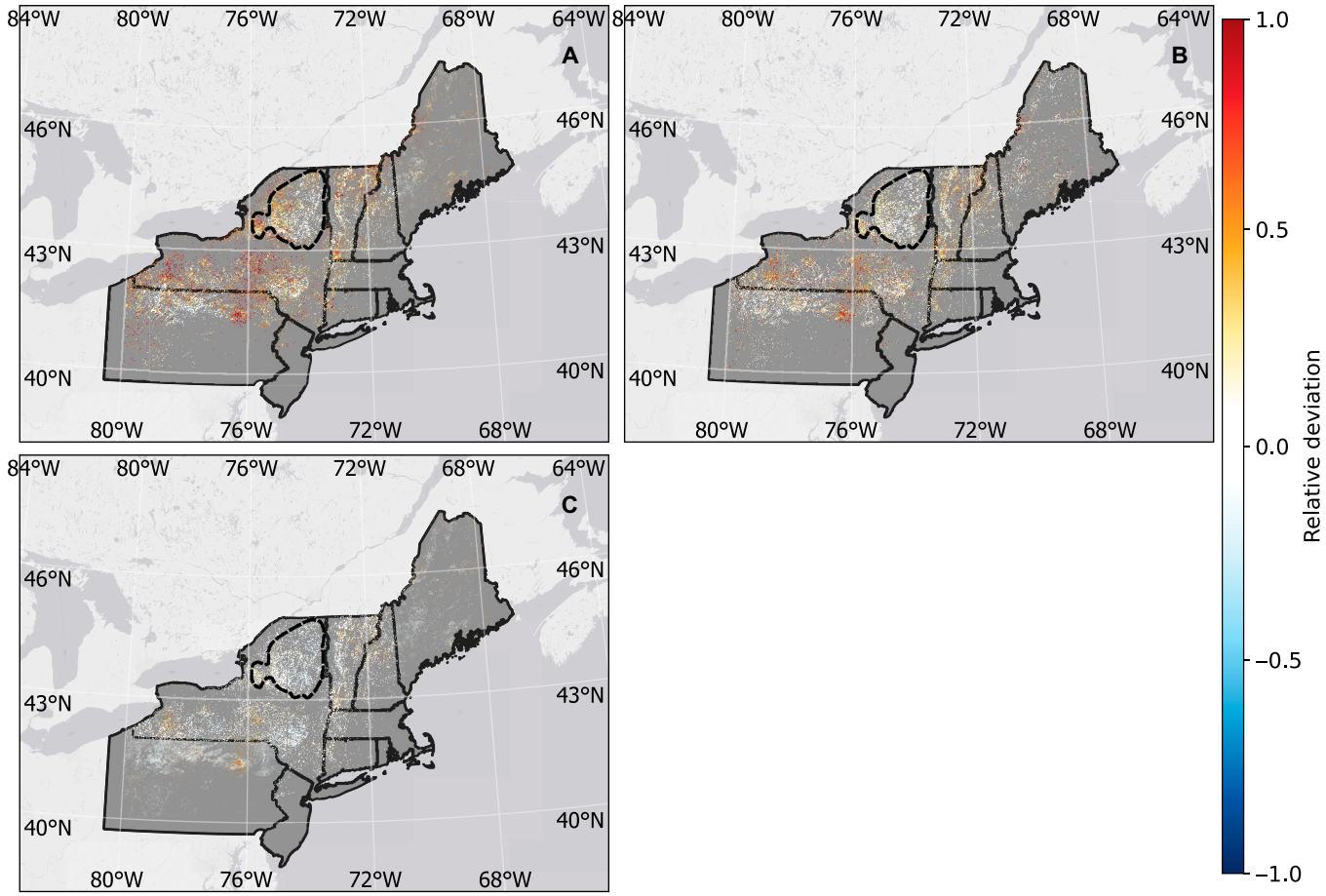

Fig. 8. Relative deviation (= (ASRL−Ref) / Ref) for no-trend pixels of the ASRL potential tree height from (A) GEDI L3, (B) Potapov et al. [46], and (C) Lang et al. [47].

We evaluated the model's sensitivity to 5 input climate variables as well as 4 selected parameters that are essential to both modules of the model (Table 4 and Figs. 9 and 10). The study area-level mean of percentage change of predicted potential tree height is calculated for every scenario in which all pixels are subject to a perturbation magnitude of a quantity. We first calculated pixel-level new height predictions and changes in percents and then obtained the spatial average over the whole study area. Sensitivity analysis confirms that inaccuracies of some quantities may affect model stability more than others. The 3 most sensitive quantities are vapor pressure, air temperature, and coefficient for canopy height-tree height allometry (β_6), which contribute to greater changes in predicted potential tree height than their own perturbation magnitudes. They are necessary to be cautious about in future model applications. The sensitivity curves for vapor pressure, temperature, and β_6 showed obvious convexity. Curves for temperature and β_6 are convex and decreasing. Compared with positive perturbations, negative perturbations have more impact on the model's predictions. This indicates that underestimates of temperature and β_6 may lead to greater uncertainty than overestimates. In contrast, for vapor pressure, the greater impact on model results occurs at positive perturbations given the convex, increasing sensitivity curve.

The model is overall more sensitive to Q_e's inputs and parameters than to Q_p's. The most sensitive quantities mentioned above all belong to the Q_e module. Sensitivity to the 3 Q_p quantities tested (precipitation, γ, and $\widetilde{h}$) are equal; a 10% perturbation brings about a 3% change in model prediction (Table 4). This level is lower than that of the Q_e quantities tested. This implies the Q_e module can be a more important concern for avoiding inaccurate model predictions.

Discussion

We deployed a water balance-based model, namely ASRL, to provide a map of potential tree height predictions for the BMB forests in the northeastern United States aiming to assist forest restoration planning. With a threshold of +20% deviation, we marked 1.21×10^6 ha of forests, or 16.7% of total forests of interest, where the predicted potential heights are greater than the existing tree height (i.e., Lang et al. [47]). Based on the masked map with the CCDC no-trend mask, nearly a half of the excessive positive deviations were explained as false errors, i.e., the forests have not reached enough maturity. The remaining half were confirmed as model overestimation. The model underestimation (of 20%) took place on 4.8×10^5 ha (6.6%).

This lightweight model consists of 2 modules. The water absorption availability module uses precipitation, topography, and root properties to estimate the tree's available water flow. The ET module, based on a big-leaf model (the Penman–Monteith equation [27]), estimates actual water consumption. Both flow rates vary with the size of the whole tree, therefore

Downloaded from https://spj.science.org on October 14, 2023

Table 4. Sensitivity analysis for input climate variables and selected model parameters.

% Change in variables	−10%	−5%	+5%	+10%
		% Change in ASRL		
Wind speed	+8.97%	+4.28%	−3.91%	−7.52%
Vapor pressure	−13.3%	−6.94%	+7.69%	+16.3%
Air temperature	+14.4%	+6.81%	−6.09%	−11.6%
SW radiation	+7.17%	+3.53%	−3.42%	−6.73%
Precipitation	−3.16%	−1.55%	+1.49%	+2.94%
% Change in parameters	−10%	−5%	+5%	+10%
		% Change in ASRL		
Single leaf area, s_{leaf}	+3.71%	+1.79%	−1.67%	−3.23%
Root absorption efficiency, γ	−3.16%	−1.55%	+1.49%	+2.94%
Coef. h_{can} versus h, β_6	+11.57%	+5.47%	−4.92%	−9.38%
Reference tree height, $\widetilde{h}$	−3.16%	−1.55%	+1.49%	+2.94%

the potential tree height is found at the point where they intersect. In the large-span area of interest, predictions of potential tree height are overall consistent with the actual tree heights in mature forests of both Ecoregion M212D and validation region, demonstrating the effectiveness and generalizability of the model, even though it does not have complex mechanisms, e.g., water potential-based plant hydraulics [50], vertical variation of light intensity in the canopy [51], and water-carbon coupling on leaves [52]. Our results imply that the task of making static predictions of potential tree height may not have to rely on overloaded dynamic processes.

Our new version endows the ASRL model with even better performance. The first version, deployed at site scale across the US, reported an overestimation magnitude of 50-100 feet ($\approx 15-30$ m) in northeastern United States and a large span of error of $\pm$100% nationwide (see Fig. 1 of Kempes et al. [20]). Compared with the first model version, the new version provides more realistic predictions for a particular species group due to improved simulation time scale, more targeted parameterization, and more complete mechanisms, and provides better spatial coverage by using gridded climate reanalysis data. Compared with the second version, it does not use the parameter tuning tactics to fit to existing tree height observations and therefore retains the prognostic nature of the original model.

Model evaluation focused on selected regions that were likely to be representative of mature forests, e.g., Ecoregion M212D and no-trend forests. This provides a large-scale perspective for interpreting the results. Using the existing tree height data to evaluate, the model performs "worse" outside Ecoregion M212D than inside it. This is largely due to deviations on immature forests outside. The presence of the positive deviation is welcomed by this work as half of them indicate possible forest restoration opportunities, which our restoration-oriented model expects to find. However, the excessively high predictions of the model in some areas cannot be entirely attributed to the conceptual mismatch between "potential" and "existing" but may be overestimations of the potential itself. In forests of higher tree height levels, the model's predictions, while overall aligning existing heights, gave even higher potential tree height estimates for some spots. This phenomenon occurs in parts of southern New York, Pennsylvania, Vermont, and New Hampshire, where forests have been growing for decades and are not subject to large-scale disturbances. A more plausible explanation is that the model overestimates the potential tree heights there. It should be noted that spatially continuous bias is highly likely to be related to the uncertainty of input. Two climate reanalysis datasets were used for the key climate input, which improves the spatial coverage of the model, but inevitably introduces more uncertainties. Sensitivity analysis confirmed that uncertainties in air temperature and humidity would cause disproportionate perturbations to the model predictions. Therefore, in future applications, it is necessary to ensure the quality of climate input data when using this model.

As to a small-scale perspective for interpreting the results, the performance of the model is strongly related to the terrain. We found a small portion of pixels whose potential tree heights were substantially underestimated (Fig. 6). Screening confirmed that underestimation was more likely to occur in mountainous terrain with higher slopes ($P < 0.05$). This phenomenon may be explained that the normalized TWI coefficient introduced in the Q_p module is not enough for perfect terrain correction. This coefficient may not drop to a low enough level on heavily sloped terrain. Our alternative explanation focuses on the Q_e module instead. Since the widespread topographic overshadows in mountainous areas are not considered, the model may mistakenly give an ET estimate of complete daytime light exposure to a site that is shadowed for part or full of day, which is an overestimate of Q_e. Such overestimation will shift the intersection of Q_e and Q_p leftward (Fig. 1), hence resulting in an underestimation of potential tree height. Future work will test both explanations with more data and experiments and apply more adjustments to the corresponding modules, but we are more inclined to attribute these errors to the latter case because the sensitivity analysis implies a greater overall impact of the Q_e module on model outputs.

The sensitivity analysis points to an unoptimistic outlook, i.e., a rising temperature and/or falling humidity, which is likely to occur with the changing climate, will contribute to the decline of potential tree height levels. This implies the shrinking of forest potential under climate change, which is the same as the conclusion of Bastin et al. [53] that was made by a fundamentally different approach. Such anticipation highlights the urgency of forest restoration efforts that are oriented to climate change mitigation.

This work was made possible by GEE Python API in that the major computing tasks were done on the cloud. GEE offers new possibilities for research and applications that require massive geographic computing, but so far, few ecological mechanism-based models have been deployed there. In this work, the ecological model was programmed in a way of image processing. Technically, that all the computation could be turned into matrix operations is an important reason why the model

Downloaded from https://spj.science.org on October 14, 2023

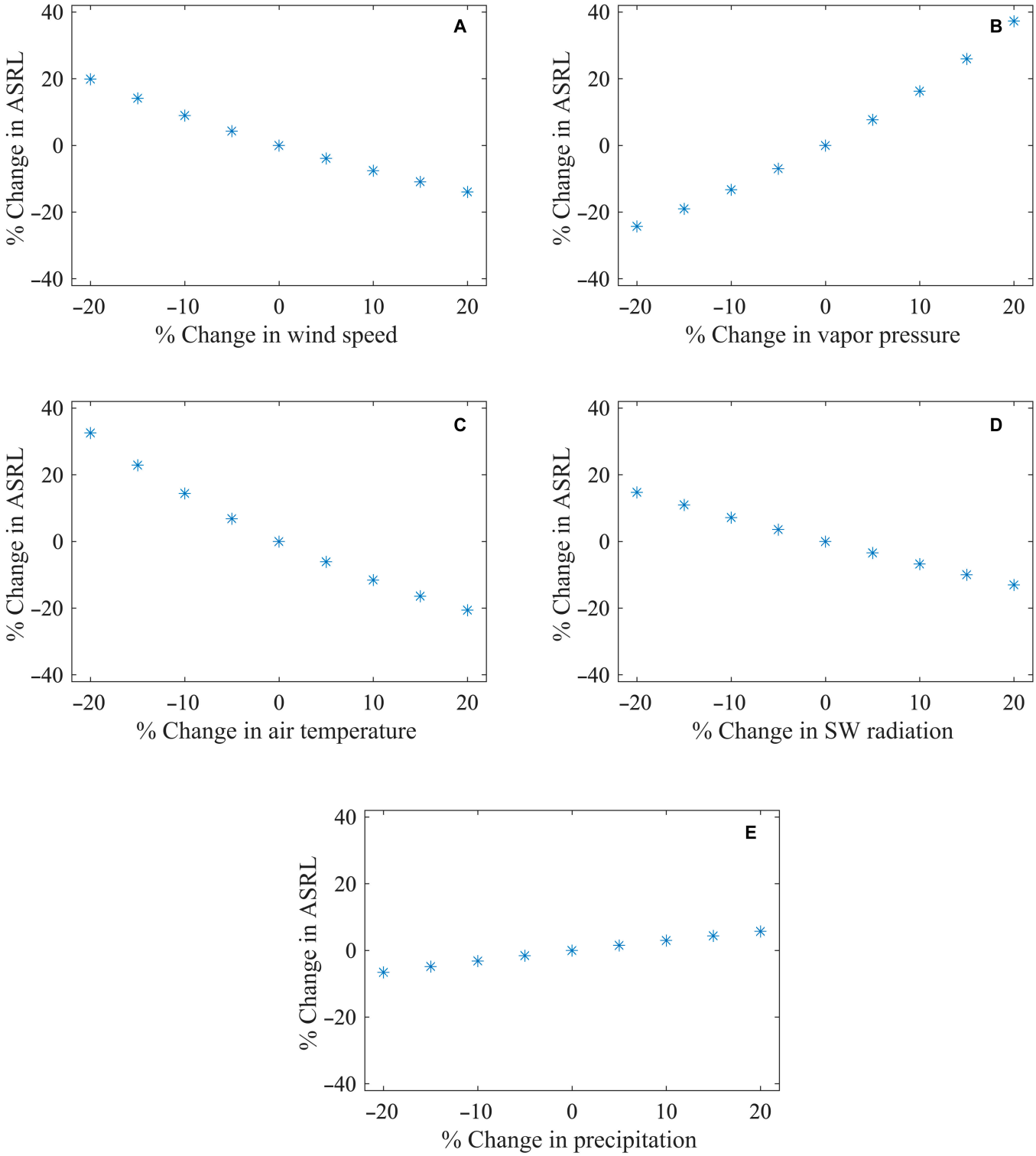

Fig. 9. Sensitivity analysis for input climate variables: (A) wind speed, (B) vapor pressure, (C) air temperature, (D) SW radiation, and (E) precipitation.

deployment could be reformatted this way. In the meantime, its simplicity avoided the use of iteration and recursion, as it included neither time-dependent processes nor plant's proactive adaptations to the environment. Those specificities made ASRL one of the few mechanism-based models that fit to requirements and limitations of GEE. Currently, we are not optimistic about GEE's capability of supporting more complex ecological models on a large span due to the task time and memory limitations. Nevertheless, we hope our work may inspire more ecologists to consider the feasibility and strategies for adapting their own models to the modern geographic cloud computing platform.

To conclude, our improved mechanism-based model provides satisfactory predictions of tree height potential for the

Downloaded from https://spj.science.org on October 14, 2023

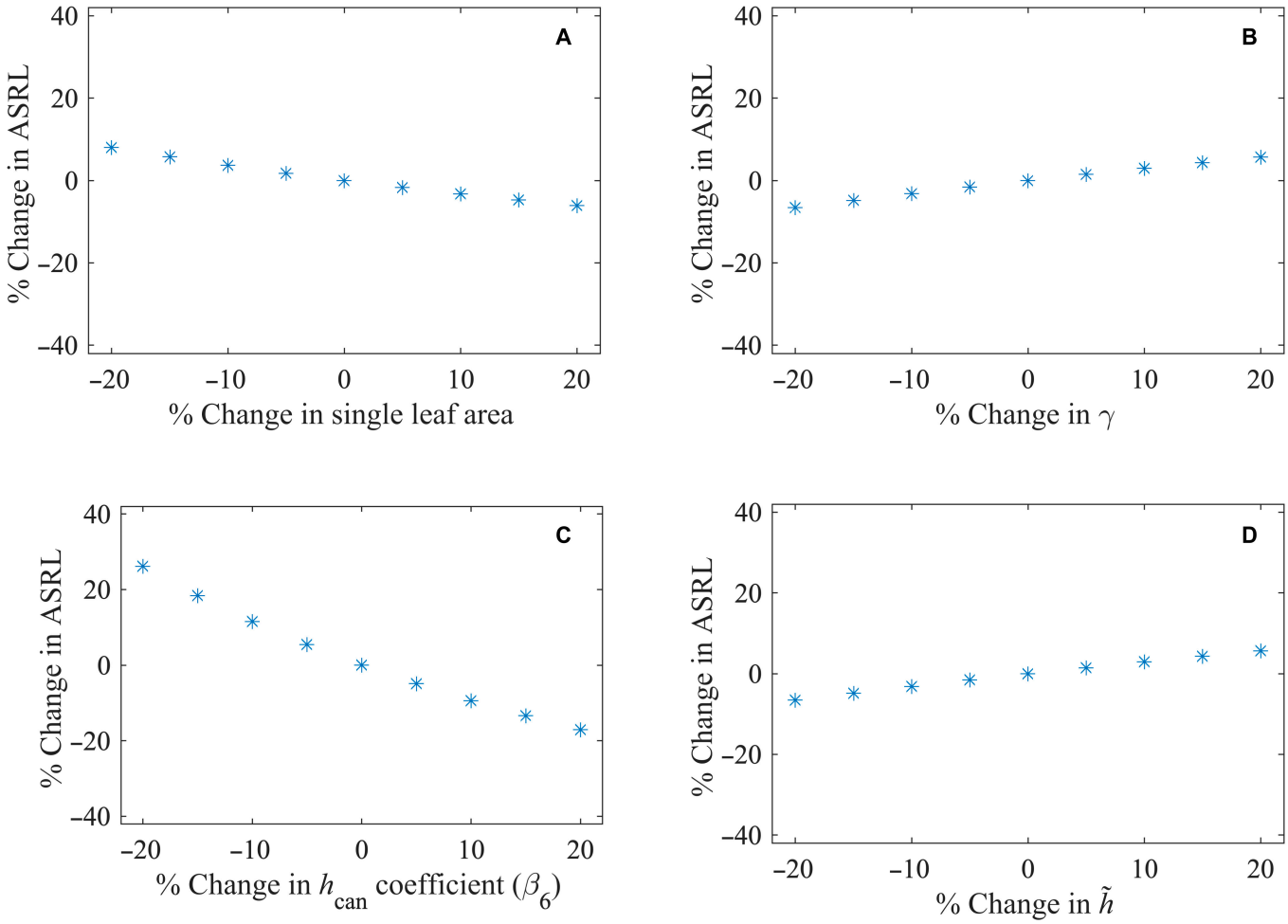

Fig. 10. Sensitivity analysis for selected model parameters: (A) single leaf area s_{leaf} (initial value 30 cm^2), (B) root absorption efficiency γ (initial value 0.12), (C) coefficient for canopy height-tree height allometry β_6 ($h_{can} = \beta_6 * h$, initial value 0.35), and (D) reference tree height (initial value 25 m).

BMB deciduous forests in northeastern United States. The improvements include finer spatial and temporal scales of water flow simulation, consideration of hydraulic limitations, and abandonment of an insufficiently verified module. The method extends the feasibility of observed allometric relationships in forest potential forecasting. Given that current understanding of forest restoration opportunities is mostly based on machine learning methods and spatially discriminatory training data, our mechanism-based model has the potential to provide considerable complement of knowledge. In future works, lessons learned in this study will be utilized to predict forest potential heights across the entire area of the United States and all species groups. Such predictive dataset will be explored to aid planning and evaluation of forest restorations.

Acknowledgments

Funding: This work is supported by the NASA Remote Sensing Theory Project [grant number 80NSSC20K1743]. **Author contributions**: The authors confirm contribution to the paper as follows: study conception and design: Z.Z. and R.B.M.; data collection: Z.Z. and L.D.; analysis and interpretation of results: Z.Z., L.D., Y.K., and R.B.M.; draft manuscript preparation: Z.Z. and L.D. All authors reviewed the results and approved the final version of the manuscript. **Competing Interests**: The authors declare that there is no conflict of interest regarding the publication of this article.

Data Availability

Estimates of potential tree height produced in this research is publicly available on GEE (image ID: "users/zpzuoBU/potential-tree-height_asrl-v3_ne-us_bmb_deciduous").
The datasets used in this research are publicly available. RTMA products provided by NOAA/NCEP are accessible on the RTMA webpage (https://www.nco.ncep.noaa.gov/pmb/products/rtma) and on GEE (collection ID: "NOAA/NWS/RTMA", see https://developers.google.com/earth-engine/datasets/catalog/NOAA_NWS_RTMA). DAYMET Version 4 product is downloadable at the NASA ORNL DAAC (https://daac.ornl.gov/cgi-bin/dsviewer.pl?ds_id=1840) and accessible on GEE (collection ID: "NASA/ORNL/DAYMET_V4", see https://developers.google.com/earth-engine/datasets/catalog/NASA_ORNL_DAYMET_V4). FIA Database Version 1.8.0.03 is downloaded from FIA DataMart (https://apps.fs.usda.gov/fia/datamart/datamart.html). Tree trait data from TRY Database are requested via the TRY website (www.try-db.org/TryWeb/Prop0.php).

Downloaded from https://spj.science.org on October 14, 2023

Supplementary Materials

Supplementary Methods
Figs. S1 to S4

References

1. DellaSala DA, Mackey B, Norman P, Campbell C, Comer PJ, Kormos CF, Keith H, Rogers B. Mature and old-growth forests contribute to large-scale conservation targets in the conterminous United States. *Fronti Forest Global Change*. 2022;5:979528.
2. Chen X, Niu J. Relationships between tree height and tree species richness at small scales. *Acta Oecol*. 2020;109:103668.
3. Feldpausch TR, Lloyd J, Lewis SL, Brienen RJW, Gloor M, Monteagudo Mendoza A, Lopez-Gonzalez G, Banin L, Abu Salim K, Affum-Baffoe K, et al. Tree height integrated into pantropical forest biomass estimates. *Biogeosciences*. 2012;9:3381.
4. Khan MNI, Islam MR, Rahman A, Azad MS, Mollick AS, Kamruzzaman M, Sadath MN, Feroz SM, Rakkibu MG, Knohl A. Allometric relationships of stand level carbon stocks to basal area, tree height and wood density of nine tree species in Bangladesh. *Global Ecol Conserv*. 2020;22:e01025.
5. King DA, Wright SJ, Connell JH. The contribution of interspecific variation in maximum tree height to tropical and temperate diversity. *J Trop Ecol*. 2006;22:11.
6. Ruiz-Benito P, Gómez-Aparicio L, Paquette A, Messier C, Kattge J, Zavala MA. Diversity increases carbon storage and tree productivity in Spanish forests: Diversity effects on forest carbon storage and productivity. *Glob Ecol Biogeogr*. 2014;23:311.
7. West GB, Brown JH, Enquist BJ. A general model for the structure and allometry of plant vascular systems. *Nature*. 1999;400(6745):664.
8. Crouzeilles R, Curran M, Ferreira MS, Lindenmayer DB, Grelle CEV, Rey Benayas JM. A global meta-analysis on the ecological drivers of forest restoration success. *Nat Commun*. 2016;7:11666.
9. Gray A, Brandeis T, Shaw J, McWilliams W, Miles P. Forest inventory and analysis database of the United States of America (FIA). *Biodiv Ecol*. 2012;4:225.
10. Dubayah R. GEDI L2B Canopy Cover and Vertical Profile Metrics Data Global Footprint Level V001; 2020.
11. Fricker GA, Synes NW, Serra-Diaz JM, North MP, Davis FW, Franklin J. More than climate? Predictors of tree canopy height vary with scale in complex terrain, Sierra Nevada, CA (USA). *For Ecol Manag*. 2019;434:142–153.
12. Niklas KJ. Maximum plant height and the biophysical factors that limit it. *Tree Physiol*. 2007;27(33):433–440.
13. Koch GW, Sillett SC, Jennings GM, Davis SD. The limits to tree height. *Nature*. 2004;428(6985):851–854.
14. Mencuccini M. Hydraulic constraints in the functional scaling of trees. *Tree Physiol*. 2002;22(8):553–565.
15. Ryan MG, Yoder BJ. Hydraulic limits to tree height and tree growth. *Bioscience*. 1997;47(4):235–242.
16. Givnish TJ, Wong SC, Stuart-Williams H, Holloway-Phillips M, Farquhar GD. Determinants of maximum tree height in *eucalyptus* species along a rainfall gradient in Victoria Australia. *Ecology*. 2014;95(11):2991–3007.
17. McMahon T. Size and Shape in Biology. *Science*. 1973;179(4079):1201–1204.
18. Ishii H, Takashima A, Makita N, Yoshida S. Vertical stratification and effects of crown damage on maximum tree height in mixed conifer-broadleaf forests of Yakushima Island, southern Japan. *Plant Ecol*. 2010;211(1):27–36.
19. Niklas KJ, Spatz H-C. Growth and hydraulic (not mechanical) constraints govern the scaling of tree height and mass. *Proc Natl Acad Sci*. 2004;101(44):15661–15663.
20. Kempes CP, West GB, Crowell K, Girvan M. Predicting maximum tree heights and other traits from allometric scaling and resource limitations. *PLoS One*. 2011;6(6):e20551.
21. Cao C, Ni X, Wang X, Lu S, Zhang Y, Dang Y, Singh RP. Allometric scaling theory-based maximum forest tree height and biomass estimation in the three gorges reservoir region using multi-source remote-sensing data. *Int J Remote Sens*. 2016;37(5):1210–1222.
22. Choi S, Ni X, Shi Y, Ganguly S, Zhang G, Duong H, Lefsky M, Simard M, Saatchi S, Lee S, et al. Allometric scaling and resource limitations model of tree heights: Part 2. Site based testing of the model. *Remote Sens*. 2013;6(5):202.
23. Choi S, Kempes CP, Park T, Ganguly S, Wang W, Xu L, Basu S, Dungan JL, Simard M, Saatchi SS, et al. Application of the metabolic scaling theory and water-energy balance equation to model large-scale patterns of maximum forest canopy height: Large-scale modeling of maximum forest height patterns. *Glob Ecol Biogeogr*. 2016;25(12):1428–1442.
24. Ni X, Park T, Choi S, Shi Y, Cao C, Wang X, Lefsky M, Simard M, Myneni R. Allometric scaling and resource limitations model of tree heights: Part 3. Model optimization and testing over continental China. *Remote Sens*. 2014;6(5):3533–3553.
25. Shi Y, Choi S, Ni X, Ganguly S, Zhang G, Duong H, Lefsky M, Simard M, Saatchi S, Lee S, et al. Allometric scaling and resource limitations model of tree heights: Part 1. Model optimization and testing over continental USA. *Remote Sens*. 2013;5(1):284–306.
26. Zhang Y, Shi Y, Choi S, Ni X, Myneni RB. Mapping maximum tree height of the great Khingan Mountain, Inner Mongolia using the Allometric scaling and resource limitations model. *Forests*. 2019;10(5):380.
27. Monteith JL, Unsworth MH. P*rinciples of environmental physics: Plants, animals, and the atmosphere*. 4th ed. Boston (MA): Elsevier/Academic Press; 2013.
28. Quinn PF, Beven KJ, Lamb R. The ln(a/tan/β) index: How to calculate it and how to use it within the TOPMODEL framework. *Hydrol Process*. 1995;9:161.
29. Kopecká M, Macek M, Wild J. Topographic wetness index calculation guidelines based on measured soil moisture and plant species composition. *Sci Total Environ*. 2021;757:143785.
30. Enquist BJ, Brown JH, West GB. Allometric scaling of plant energetics and population density. *Nature*. 1998;395:163–165.
31. Sperry JS, Smith DD, Savage VM, Enquist BJ, McCulloh KA, Reich PB, Bentley LP, von Allmen EI. A species-level model for metabolic scaling in trees I. exploring boundaries to scaling space within and across species. *Funct Ecol*. 2012;26(5):1054–1065.
32. Campbell GS, Norman JM. *Introduction to environmental biophysics*, 2nd ed. New York (NY): Springer; 1998.
33. Ruefenacht B, Finco MV, Nelson MD, Czaplewski R, Helmer EH, Blackard JA, Holden GR, Lister AJ, Salajanu D, Weyermann D, et al. Conterminous U.S. and Alaska forest type mapping using Forest inventory and analysis data. *Photogramm Eng Remote Sens*. 2008;74:1379.
34. Dewitz J. National Land Cover Database (NLCD) 2019 Products; 2021.

Downloaded from https://spj.science.org on October 14, 2023

35. Bailey RG. *Bailey's ecoregions and subregions of the United States*, Puerto Rico, and the U.S, Virgin Islands; 2016.
36. Besnard S, Koirala S, Santoro M, Weber U, Nelson J, Gütter J, Herault B, Kassi J, N'Guessan A, Neigh C, et al. Mapping global forest age from forest inventories, biomass and climate data. *Earth Syst Sci Data*. 2021;13:4881.
37. Lehner B, Verdin K, Jarvis A. New global hydrography derived from Spaceborne elevation data. *EOS Trans Am Geophys Union*. 2008;89(10):93–104.
38. Mattivi P, Franci F, Lambertini A, Bitelli G. TWI computation: A comparison of different open source GISs. *Open Geospat Data, Softw Stand*. 2019;4(1):6.
39. De Pondeca MSFV. The real-time mesoscale analysis at NOAA's National Centers for environmental prediction: Current status and development. *Weather Forecast*. 2011;26(5):593–612.
40. Thornton M. Daymet: *Daily surface weather data on a 1-km grid for North America*, Version 4 p. 0 MB (2020). Artwork Size: 0 MB Medium: netCDF Publisher: ORNL Distributed Active Archive Center Version Number: 4.
41. Cavender-Bares J, Keen A, Miles B. Phylogenetic structure of floridian plant communities depends on taxonomic and spatial scale. *Ecology*. 2006;87(7 Suppl):S109–S122.
42. Kattge J, Bönisch G, Díaz S, Lavorel S, Prentice IC, Leadley P, Tautenhahn S, Werner GDA, Aakala T, Abedi M, et al. TRY plant trait database - enhanced coverage and open access. *Glob Chang Biol*. 2020;26(1):119–188.
43. Messier J. *Megantic-Trait-Data: Mont_mégantic_individual_traits_2016-2017*; 2019.
44. Messier J, Violle C, Enquist BJ, Lechowicz MJ, McGill BJ. Similarities and differences in intrapopulation trait correlations of co-occurring tree species: Consistent water-use relationships amid widely different correlation patterns. *Am J Bot*. 2018;105(9):1477–1490.
45. Shipley B, Vu T-T. Dry matter content as a measure of dry matter concentration in plants and their parts. *New Phytol*. 2002;153(2):359–364.
46. Potapov P, Li X, Hernandez-Serna A, Tyukavina A, Hansen MC, Kommareddy A, Pickens A, Turubanova S, Tang H, Silva CE, et al. Mapping global forest canopy height through integration of GEDI and Landsat data. *Remote Sens Environ*. 2021;253(4):112165.
47. Lang N, Jetz W, Schindler K, Wegner JD, A high-resolution canopy height model of the Earth. arXiv. 2022. https://doi.org/10.48550/arXiv.2204.08322
48. Chen S, Olofsson P, Saphangthong T, Woodcock CE. Monitoring shifting cultivation in Laos with Landsat time series. *Remote Sens Environ*. 2023;288:113507.
49. Zhu Z, Woodcock CE. Continuous change detection and classification of land cover using all available Landsat data. *Remote Sens Environ*. 2014;144:152.
50. Kennedy D, Swenson S, Oleson KW, Lawrence DM, Fisher R, Lola da Costa AC, Gentine P. Implementing plant hydraulics in the community land model, version 5. *J Adv Model Earth Syst*. 2019;11(2):485–513.
51. Thornley JHM. Instantaneous canopy photosynthesis: Analytical expressions for sun and shade leaves based on exponential light decay down the canopy and an acclimated non-rectangular hyperbola for leaf photosynthesis. *Ann Bot*. 2002;89(4):451–458.
52. Tuzet A, Perrier A, Leuning R. A coupled model of stomatal conductance, photosynthesis and transpiration: Coupled model of stomatal conductance, photosynthesis and transpiration. *Plant Cell Environ*. 2003;26(7):1097–1116.
53. Bastin J-F, Finegold Y, Garcia C, Mollicone D, Rezende M, Routh D, Zohner CM, Crowther TW. The global tree restoration potential. *Science*. 2019;365(6448):76–79.

Downloaded from https://spj.science.org on October 14, 2023